JOURNAL OF Materials CHEMISTRY

# Ground state phases and optical properties in extended Peierls–Hubbard models for halogen-bridged binuclear metal complexes†

**Makoto Kuwabara**[a] **and Kenji Yonemitsu***[a,b]

[a]*Department of Theoretical Studies, Institute for Molecular Science, Myodaiji, Okazaki 444-8585, Japan. E-mail: kxy@ims.ac.jp*
[b]*Department of Functional Molecular Science, Graduate University for Advanced Studies, Myodaiji, Okazaki 444-8585, Japan*

***Received 28th February 2001, Accepted 9th May 2001***
***First published as an Advance Article on the web 11th July 2001***

Mechanisms of a variety of charge and lattice ordered phases observed in halogen-bridged binuclear metal complexes are theoretically studied by applying the exact diagonalization and strong-coupling expansion methods to one- and two-band extended Peierls–Hubbard models. In $R_4[Pt_2(pop)_4I]nH_2O$ [R = Na, K, $NH_4$, $(CH_3(CH_2)_7)_2NH_2$, *etc.*, pop = $P_2O_5H_2^{2-}$] containing charged MMX chains, three electronic phases are suggested by experiments. We find that the variation of the electronic phases originates not only from competition between site-diagonal electron–lattice and electron–electron interactions but also from competition between short-range and long-range electron–electron interactions. On the other hand, in $Pt_2(RCS_2)_4I$ (R = $CH_3$, *n*-$C_4H_9$) containing neutral MMX chains, a site-off-diagonal electron–lattice interaction and the absence of counter ions are found to be crucial to produce the recently found, ordered phase. The optical conductivity spectra are also studied, which directly reflect the electronic phases. Their dependence on the electronic phase and on model parameters is clarified from the strong-coupling viewpoint.

## Introduction

Metal complexes of low-dimensional electronic and crystal structures have attracted much interest from both chemists and physicists. Among these, quasi-one-dimensional halogen-bridged metal complexes have strong electron–lattice and electron–electron interactions. These interactions compete with each other to produce a variety of electronic phases. The electronic properties depend on transition metal (M) atoms, halogen (X) atoms, ligands, and counter ions. Mononuclear metal complexes contain chains consisting of repeating MX units and are called MX chains. Binuclear metal complexes have chains consisting of repeating MMX units and are called MMX chains. The electronic phases of the MX chains are classified into an averaged-valence phase for M = Ni and a mixed-valence phase for M = Pt and Pd. The former phase is often called a Mott–Hubbard phase, and the latter a charge-density-wave phase. Both phases are insulating. The MX chains have been studied experimentally and theoretically for some time.[1]

Meanwhile, studies of MMX chains are still actively ongoing and novel electronic phases are being discovered. Observed and suggested electronic phases for MMX chains are schematically shown in Fig. 1 and classified into an averaged-valence (AV) phase, a charge-density-wave (CDW) phase, a charge-polarization (CP) phase, and an alternate-charge-polarization (ACP) phase. From the valences of the metal atoms, the CDW, CP, and ACP phases are also called the 2233, 2323, and 2332 phases, respectively. Because electrons are not completely localized, the formal valences 2 and 3 mean valences $2.5-\delta$ and $2.5+\delta$, in reality, with $0<\delta<0.5$. The AV and CP phases are paramagnetic, while the CDW and ACP phases are nonmagnetic. In the CDW phase, the spin gap is expected to be comparable with the charge gap. Meanwhile, in the ACP phase, the spin gap is generally much smaller than the charge gap. In principle, all of the four phases are insulating because of the finite charge gap.

In this paper, we consider compounds with M = Pt. There are two classes of MMX chains. i) In $R_4[Pt_2(pop)_4X]nH_2O$ with monovalent cations R, four ligands of pop = $P_2O_5H_2^{2-}$ surround the binuclear unit. Compounds with X = Cl and Br are well characterized. The ground states of $K_4[Pt_2(pop)_4X]$-$nH_2O$ with X = Cl and Br are known to be in the CDW phase.[2–5] Meanwhile, compounds with X = I have recently been studied extensively and show different electronic phases.[6–8] The

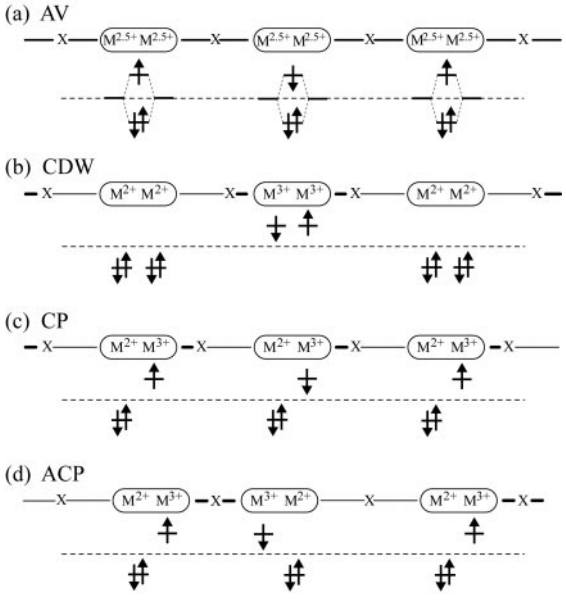


**Fig. 1** Schematic electronic and lattice structures of MMX chains.

†Electronic supplementary information (ESI) available: ground-state phase diagrams of the 18-site two band model for infinitely large $K_{MXM}$ and for $K_{MXM}=0$. See http://www.rsc.org/suppdata/jm/b1/b101545l/

DOI: 10.1039/b101545l

mechanism of the variation of the electronic phases is clarified in this paper. ii) In $Pt_2(RCS_2)_4I$, the ligands surrounding the binuclear unit are $RCS_2$ with $R=CH_3$, $C_2H_5$, $n$-$C_4H_9$, *etc.* Among these, the compound with $R=CH_3$ (the ligand is then dta $=CH_3CS_2$) has been studied for many years[9] and has been found to show the AV phase with "metallic" conductivity above room temperature.[10,11] The compound with $R=n$-$C_4H_9$ clearly shows the ACP phase.[12] The difference between the pop and dta systems is discussed from the theoretical viewpoint in this paper.

Among the four phases mentioned above, the AV phase has the smallest charge gap and the best electric conductivity because electron correlation, more precisely the Mott mechanism, is the origin of the insulating ground state. It is true that the more degrees of freedom, compared with those in the MX chains, are responsible for the greater variety of electronic phases in the MMX chains, but the smaller charge gap appears to enhance the controllability of relative stability among the four phases above. As a consequence, electrons are more delocalized than in the MX chains. Among the four phases observed or suggested in the MMX chains, the CP and ACP phases are new and have not been realized in the MX chains. The ACP phase is regarded as a spin-Peierls phase because the spin gap is produced by dimerization of the binuclear units. The CP phase is, on the other hand, quite new. It is accompanied by lattice distortion, but it is paramagnetic. These characteristics are usually incompatible with each other. Furthermore, the inversion symmetry is spontaneously broken to have charge polarization, so that ferroelectricity is generally expected, although it has not yet been observed. This quite new phase is realized because of a subtle balance between electron–lattice and electron interactions, as explained in this paper.

Most of the theoretical studies into the origins of the charge and lattice orders in the MMX chains are rather new. First, extended Hückel band structure calculations were performed.[13,14] Electron–electron interactions are, in principle, incorporated into renormalized transfer integrals only. The Hartree–Fock approximation is applied to one-dimensional, two-band[15,16] and one-band[17,18] extended Peierls–Hubbard models. Recently, the Hartree–Fock calculations are extended to finite-temperature systems.[19] These calculations capture the qualitative aspect of the electronic origin of each phase, but miss quantum fluctuations that are inherent in one-dimensional electron systems. Recently, the quantum fluctuations originating from electron correlation in these models have been quantitatively taken into account by using the exact diagonalization method[20,21] and the quantum Monte Carlo method.[22] In this paper, we quantitatively treat the electron correlation by using the exact diagonalization method and analyze the numerical results with second- and fourth-order perturbation theories from the strong-coupling limit. Then, the optical conductivity spectra are calculated in one- and two-band models for the MMX chains as well as XMMX monomers. It will be found that these calculations are useful to evaluate model parameters and to understand the ground and photoexcited states systematically. We discuss in detail the relevance of our theoretical results to the experimentally observed variation of the ground and photoexcited states.

## Extended Peierls–Hubbard models

To describe the ground- and excited-state properties, we adopt extended Peierls–Hubbard models, which are schematically shown in Fig. 2. The simpler one shown in the upper panel takes only M $d_{z^2}$ orbitals into account and is called the one-band model. Their energy levels and transfer integrals depend on the positions of the X ions,

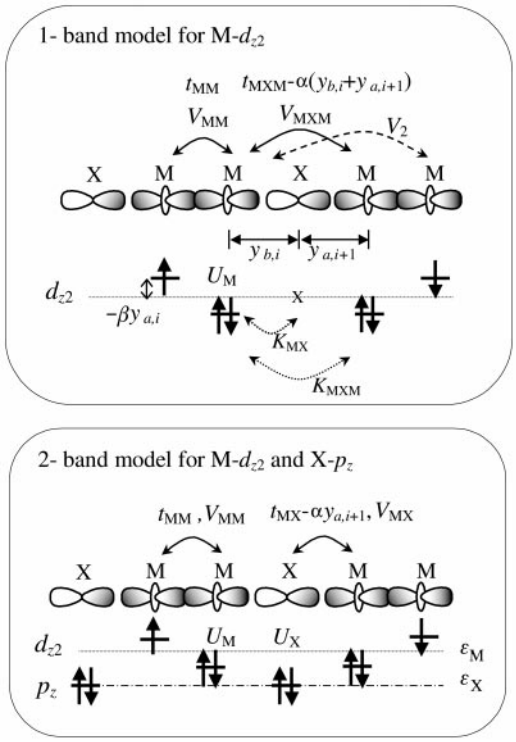


**Fig. 2** One- and two-band models for the MMX chains.

$$
\begin{aligned}
H_1 = & -\sum_{i,\sigma} t_{MM}(c^{+}_{a,i,\sigma}c_{b,i,\sigma}+\text{h.c.}) \\
& -\sum_{i,\sigma}[t_{MXM}-\alpha(y_{b,i}+y_{a,i+1})](c^{+}_{b,i,\sigma}c_{a,i+1}+\text{h.c.}) \\
& -\beta\sum_{i}(y_{a,i}n_{a,i}+y_{b,i}n_{b,i}) \\
& +U_M\sum_{i}(n_{a,i,\uparrow}n_{a,i,\downarrow}+n_{b,i,\uparrow}n_{b,i,\downarrow}) \\
& +\sum_{i}(V_{MM}n_{a,i}n_{b,i}+V_{MXM}n_{b,i}n_{a,i+1}) \\
& +V_2\sum_{i}(n_{a,i}n_{a,i+1}+n_{b,i}n_{b,i+1}) \\
& +(K_{MX}/2)\sum_{i}(y^2_{a,i}+y^2_{b,i}) \\
& +(K_{MXM}/2)\sum_{i}(y_{b,i}+y_{a,i+1})^2
\end{aligned}
$$

where $c^{+}_{a,i,\sigma}$ ($c^{+}_{b,i,\sigma}$) creates an electron with spin $\sigma$ at site $a$ ($b$) in the $i$th binuclear unit, h.c. denotes hermitian conjugate, $n_{a,i,\sigma}=c^{+}_{a,i,\sigma}c_{a,i,\sigma}$ ($n_{b,i,\sigma}=c^{+}_{b,i,\sigma}c_{b,i,\sigma}$) are the number operators, and $n_{a,i}=\Sigma_\sigma n_{a,i,\sigma}$ ($n_{b,i}=\Sigma_\sigma n_{b,i,\sigma}$). The unit cell contains two M sites, $a$ and $b$, and an X site. The distance between the M site $a$ ($b$) in the $i$th unit and its neighboring X site, relative to that in the undistorted structure, is denoted by $y_{a,i}$ ($y_{b,i}$). Thus, the change in the distance between the $i$th and $(i+1)$th units is given by $y_{b,i}+y_{a,i+1}$. The nearest-neighbor transfer integral within the unit is fixed at $t_{MM}$. Meanwhile, the nearest-neighbor transfer integral through the X $p_z$ orbital, $t_{MXM}$, is assumed to be linearly modified by the length change $y_{b,i}+y_{a,i+1}$ with coefficient $\alpha$. The energy level of the M $d_{z^2}$ orbital is assumed to depend linearly on the change in the MX bond length with coefficient $\beta$. The repulsion strengths are denoted by $U_M$ for the on-site pair of electrons with opposite spins, $V_{MM}$ for the nearest-neighbor pairs within the unit, $V_{MXM}$ for the nearest-neighbor pairs accompanied with an X site in-between, and $V_2$ for the next-nearest-neighbor pairs. They are not assumed to depend on the positions of the X ions

for simplicity. The elastic constants are denoted by $K_{MX}$ for the MX bond length, and $K_{MXM}$ for the distance between the neighboring binuclear units. The latter constant is needed when counter ions hinder the units from being displaced.

The other model we use for the MMX chains takes M $d_{z^2}$ and X $p_z$ orbitals into account. It is called the two-band model,

$$\begin{aligned}H_2 = &-\sum_{i,\sigma}(t_{MX}-\alpha y_{a,i})(p^+_{i,\sigma}d_{a,i,\sigma}+\text{h.c.})\\ &-\sum_{i,\sigma}t_{MM}(d^+_{a,i,\sigma}d_{b,i,\sigma}+\text{h.c.})\\ &-\sum_{i,\sigma}(t_{MX}-\alpha y_{b,i})(d^+_{b,i,\sigma}p_{i+1,\sigma}+\text{h.c.})\\ &+\sum_i[\varepsilon_X n^p_i+(\varepsilon_M-\beta y_{a,i})n^d_{a,i}+(\varepsilon_M-\beta y_{b,i})n^d_{b,i}]\\ &+U_X\sum_i n^p_{i,\uparrow}n^p_{i,\downarrow}+U_M\sum_i(n^d_{a,i,\uparrow}n^d_{a,i,\downarrow}+n^d_{b,i,\uparrow}n^d_{b,i,\downarrow})\\ &+\sum_i(V_{MX}n^p_i n^d_{a,i}+V_{MM}n^d_{a,i}n^d_{b,i}+V_{MX}n^d_{b,i}n^p_{i+1})\\ &+(K_{MX}/2)\sum_i(y^2_{a,i}+y^2_{b,i})\\ &+(K_{MXM}/2)\sum_i(y_{b,i}+y_{a,i+1})^2\end{aligned}$$

where $p^+{}_{i,\sigma}$, $d^+{}_{a,i,\sigma}$, and $d^+{}_{b,i,\sigma}$ create an electron with spin $\sigma$ at the X, $a$(M), and $b$(M) sites, respectively, of the $i$th –X–M–M– unit, h.c. denotes hermitian conjugate, $n^p{}_{i,\sigma}=p^+{}_{i,\sigma}p_{i,\sigma}$, $n^d{}_{a,i,\sigma}=d^+{}_{a,i,\sigma}d_{a,i,\sigma}$, and $n^d{}_{b,i,\sigma}=d^+{}_{b,i,\sigma}d_{b,i,\sigma}$ are the number operators, $n^p{}_i=\Sigma_\sigma n^p{}_{i,\sigma}$, $n^d{}_{a,i}=\Sigma_\sigma n^d{}_{a,i,\sigma}$, and $n^d{}_{b,i}=\Sigma_\sigma n^d{}_{b,i,\sigma}$. The changes in the MX bond lengths, $y_a$, and $y_b$, are the same as defined in the one-band model. Note, however, the meaning of the coefficient $\alpha$ is different from that in the one-band model. That is, in the present two-band model, the transfer integral between the nearest-neighbor M $d_{z^2}$ and X $p_z$ orbitals, $t_{MX}$ (not $t_{MXM}$), is assumed to be linearly modified by the MX bond length change with coefficient $\alpha$. The meanings of the parameters $t_{MM}$, $\beta$, $U_M$, $V_{MM}$, $K_{MX}$, and $K_{MXM}$ are the same as in the one-band model. The energy level of the X $p_z$ orbital is denoted by $\varepsilon_X$, and that of the M $d_{z^2}$ orbital by $\varepsilon_M$. The one-site repulsion strength at X sites is denoted by $U_X$. The repulsion strength between the electrons at nearest-neighbor M and X sites is denoted by $V_{MX}$. Here, we drop the $V_{MXM}$ and $V_2$ terms for simplicity since the model already contains many parameters. The two-band model is reduced to the one-band model in the limit of infinitely large $\varepsilon_M-\varepsilon_X$, where all the X $p_z$ orbitals are completely occupied.

In both of the models above, the periodic boundary condition is imposed. The electronic ground state is determined by the exact diagonalization method. The lattice displacements $y_a$ and $y_b$ are treated as classical variables and determined in a self-consistent manner with the electronic ground state, unless otherwise stated, so that the system is in the lowest-energy configuration.

## Kinetic *vs.* interaction terms

Electronic phases of $R_4[Pt_2(pop)_4I]nH_2O$ [R = Na, K, $NH_4$, $(CH_3(CH_2)_7)_2NH_2$, *etc.*, pop = $P_2O_5H_2^{2-}$] are suggested to be classified according to the distance between the nearest-neighbor M atoms accompanied with an X atom in-between, $d_{MXM}$.[8] In order to study the effects of changing $d_{MXM}$, we first obtain ground-state phase diagrams by varying $t_{MXM}$ in the one-band model. Considering these pop systems containing charged MMX chains and counter ions, we set $K_{MXM}$ to be infinitely large, prohibiting displacements of M atoms and allowing displacements of X atoms only. The site-off-diagonal electron–lattice coupling $\alpha$ is then irrelevant. As a consequence, the ACP phase is not realized here. In addition, leaving detailed studies of competition among the charge-ordered phases until later, we simply neglect the long-range interactions. Exactly diagonalizing the one-band model, we show a phase diagram in the space spanned by $t_{MXM}$, $\beta$, and $U_M$ in Fig. 3, where $t_{MM}$ is set to be unity. Because the parameter sets ($\alpha$, $\beta$, $K_{MX}$, $K_{MXM}$) and ($\lambda\alpha$, $\lambda\beta$, $\lambda^2K_{MX}$, $\lambda^2K_{MXM}$) are related by the scaling of $y_a$ and $y_b$ and thus equivalent, the specific value of $K_{MX}$ is insignificant. First of all, $t_{MXM}$ is found to stabilize the AV phase. In $R_4[Pt_2(pop)_4I]nH_2O$, where electrons are the most delocalized among X = Cl, Br, and I, the AV phase may appear for small $d_{MXM}$ because $t_{MXM}$ is expected to become large. Meanwhile $t_{MXM}$ does not much affect the boundary between the CDW and CP phases. We show later that this boundary is more sensitive to $t_{MM}$.

## Electron–lattice *vs.* electron–electron interactions

In Fig. 3, the CDW phase is stabilized by the site-diagonal electron–lattice coupling $\beta$, while the CP phase is stabilized by the on-site repulsion $U_M$. Thus, the competition between the electron–lattice and electron–electron interactions determines the relative stability of these two charge-ordered phases. This fact is easily understood with the help of the second-order perturbation theory from the strong-coupling limit, $t_{MM}=t_{MXM}=\alpha=0$. The energies of the CDW and CP phases are degenerate in the limit when the long-range interactions are absent. Namely, their energies are both given by $-\beta|y|+U_M+K_{MX}y^2$ per binuclear unit. Though the effects of the long-range interactions are discussed later, it is here noted that $V_{MM}$ increases the energy of the CDW phase and stabilizes the CP phase. The second-order processes with respect to $t_{MM}$ shown

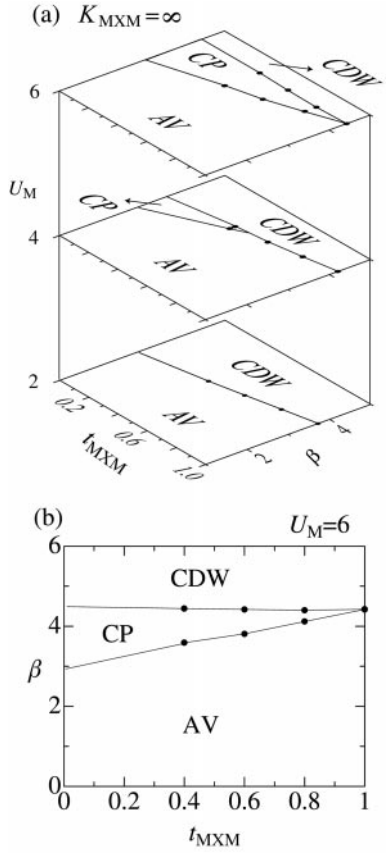


**Fig. 3** Ground-state phase diagram of the 12-site one-band model for infinitely large $K_{MXM}$, (a) in the $t_{MXM}$–$\beta$–$U_M$ space, and (b) its cross section at $U_M=6$. The parameters are $t_{MM}=1$, $\alpha=0$, $K_{MX}=6$, $V_{MM}=0$, $V_{MXM}=0$, and $V_2=0$.

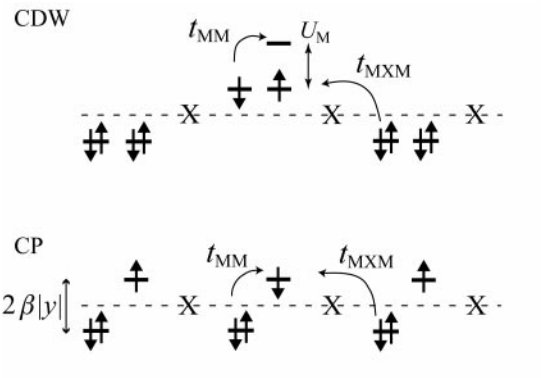


**Fig. 4** Second-order processes with respect to $t_{MM}$ and $t_{MXM}$ in the CDW and CP phases.

in Fig. 4 lower the energy by $t_{MM}^2/U_M$ in (the spin-polarized state, or by $2t_{MM}^2/U_M$ in the spin-singlet state, of) the CDW phase, and by $t_{MM}^2/(2\beta|y|)$ in the CP phase. That is why the CDW phase is relatively stable for large $\beta$, and the CP phase for large $U_M$. In a similar manner, the effect of $t_{MXM}$ can be discussed from the second-order perturbation theory. It does not affect the relative stability between the CDW and CP phases. That is why the phase boundary is insensitive to $t_{MXM}$. It is noted that, if the long-range interactions are included, the second-order terms with respect to $t_{MXM}$ for the CDW and CP phases become different, as presented later just before the optical conductivity in the one-band model. Even in such a case, the phase boundary is more sensitive to $t_{MM}$.

Experimentally, the ground states of $K_4[Pt_2(pop)_4X]nH_2O$ with X = Cl, Br and $n = 2$, 3 are shown to be in the CDW phase.[2–5] In general, when the halogen atom X is either Cl or Br, so far all the ground states are known to be in the CDW phase. For X = Cl and Br, the X $p_z$ level is so deep that the nearest-neighbor transfer integral through the X $p_z$ orbital is effectively given by $t_{MXM} \sim t_{MX}^2/(\varepsilon_M - \varepsilon_X + U_M - U_X)$ in terms of the two-band model. Because of large $\varepsilon_M - \varepsilon_X$, the transfer integral $t_{MXM}$ is expected to be small. Meanwhile, the site-diagonal electron–lattice coupling $\beta$ is expected to be large owing to the short distance between the neighboring M and X atoms, $d_{MX}$. Thus, the CDW phase for X = Cl and Br is understood from the dominance of the electron–lattice coupling $\beta$ over the electron–electron interactions, though the on-site repulsion $U_M$ is still strong enough to suppress a phase with bipolarons discussed later.

In $R_4[Pt_2(pop)_4X]nH_2O$ with X = I, depending on the cation R and on the number of water molecules $n$, three electronic phases are suggested to appear: the AV phase, the CDW phase, and the CP phase in the order of increasing $d_{MXM}$.[8] Though we have not obtained a phase diagram with the CDW phase between the other two phases, we believe that, for small $d_{MXM}$, the effect of $t_{MXM}$ is larger than those of various interactions, so that the larger $t_{MXM}$ stabilizes the AV phase. Meanwhile, for intermediate to large $d_{MXM}$, the competition between the electron–lattice and electron–electron interactions discussed here and/or the competition between the short–range and long-range electron–electron interactions discussed later determine the relative stability between the CDW and CP phases. As $d_{MXM}$ increases, the site-diagonal electron–lattice coupling $\beta$ becomes weak, while the on-site repulsion $U_M$ would not change so much. If the two phases compete with each other, then the effect of $\beta$ dominates for intermediate $d_{MXM}$ and that of $U_M$ for large $d_{MXM}$. This partially explains why the CDW phase appears for intermediate $d_{MXM}$ and the CP phase is suggested for large $d_{MXM}$. This variation of the charge-ordered phases can be explained also by the competition between the short-range and long-range electron–electron interactions, as discussed below.

## Short-range *vs.* long-range electron–electron interactions

Here, the long-range interactions, $V_{MM}$, $V_{MXM}$ and $V_2$, are included. The competition is easily understood in the strong-coupling limit, $t_{MM} = t_{MXM} = \alpha = 0$. The contribution from each interaction term to the total energy per binuclear unit is listed on the right-hand side of Fig. 5. The bond-charge-density-wave (BCDW) phase is introduced at the top here just to explain the competition. Charge ordering is formally represented by $-M^{2+}M^{4+}=X-M^{2+}M^{2+}-X-$ there. Both the bond-charge and (site-)charge densities are modulated in this phase. If the site-diagonal electron–lattice coupling $\beta$ is so strong that it dominates over the on-site repulsion $U_M$, the BCDW phase is stable, forming a bipolaron lattice. The energy gain from the electron–lattice coupling $\beta$ is the largest, approximately given by $3\beta|y|$ per unit, though the magnitudes of the lattice displacements are not uniform in the lowest-energy configuration. In any case, the BCDW phase is not experimentally observed probably because it is destabilized by the strong on-site repulsion $U_M$. The energy loss is also the largest, $(3/2)U_M$. For a fixed magnitude of the lattice displacements, all of the CDW, ACP, and CP phases gain energy by $\beta|y|$ and lose it by $U_M$. Then, the long-range interactions differentiate their energies. The CDW phase loses energy by $(5/2)V_{MM}$, the ACP phase by $(5/2)V_{MXM}$, and the CP phase by $5V_2$. Otherwise, the energy loss is given by $2V_{MM} + 2V_{MXM} + 4V_2$. When the nearest-neighbor repulsion within the unit $V_{MM}$ is dominant, the CDW phase is unstable. As the dominant interaction becomes longer-ranged, the ACP phase and finally the CP phase become unstable. Since we reasonably expect $U_M > V_{MM} > V_{MXM} > V_2$, the CP phase is the most stable in the strong-coupling limit if $\beta$ is weak enough.

In $R_4[Pt_2(pop)_4I]nH_2O$, the CDW phase appears for intermediate $d_{MXM}$, and the CP phase is suggested for large $d_{MXM}$.[8] First of all, it is unreasonable to assume that only $V_{MXM}$ is small and that the other repulsion strengths including $V_2$ are large enough to stabilize the ACP phase. Indeed, as far as $K_{MXM}$ is infinitely large, the ACP phase was not realized in our calculations. As $d_{MXM}$ increases, the next-nearest-neighbor

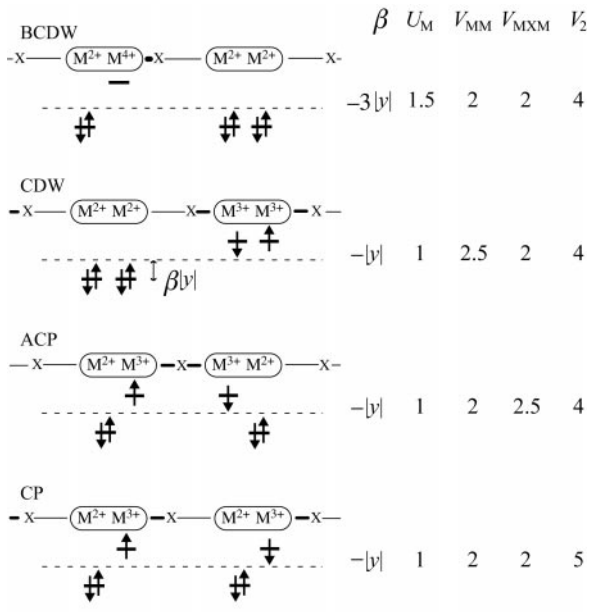


**Fig. 5** Schematic structures of the electronic phases and the coefficients of their partial energies per binuclear unit with respect to site-diagonal electron–lattice coupling $\beta$, on-site repulsion $U_M$, nearest-neighbor repulsion $V_{MM}$, $V_{MXM}$, and next-nearest-neighbor repulsion $V_2$, in the strong-coupling limit.

repulsion $V_2$ would become weak. Meanwhile, the distance between the nearest-neighbor M atoms within the unit is almost unchanged, so that the corresponding nearest-neighbor repulsion $V_{MM}$ would not change so much in comparison with $V_2$. Then, as $d_{MXM}$ increases, the CP phase becomes more stable relative to the CDW phase. This would be the other reason why the CDW phase is changed into the CP phase with increasing $d_{MXM}$. So far, we have limited the discussions to the case of infinitely large $K_{MXM}$, prohibiting displacements of M atoms and keeping $d_{MXM}$ constant.

Before going to the next section, we point out similarities in the electronic phases of the MMX chains and those of the quasi-one-dimensional organic conductors, $(TMTTF)_2X$ ($X=PF_6$, Br) and $(TMTSF)_2X$ ($X=PF_6$, $ClO_4$).[23,24] In these organic conductors, TMTTF and TMTSF molecules are crystallographically dimerized. If we neglect the dimerization, the π band is 3/4-filled in the electron picture, or 1/4-filled in the hole picture. Electron–lattice interactions are generally believed to be weak [though they are necessary in the spin-Peierls phase of $(TMTTF)_2PF_6$] in comparison with electron–electron interactions. Then, the quasi-one-dimensional organic conductors correspond to the MMX chains without lattice distortion. In these organic conductors, the dependence of physical properties on the donor molecule or on the anion can be understood as an effect of chemical pressure. On the low-"pressure" side containing $(TMTTF)_2X$, the systems are well described by one-dimensional models especially at low temperatures. In $(TMTTF)_2Br$, the ground state is an antiferromagnet accompanied by a $4k_F$ charge-density wave: the charge densities are modulated as rich, poor, rich, poor, … (period 2) as in the CP phase of the MMX chains. On the high-"pressure" side containing $(TMTSF)_2X$, the dimerization becomes weak and the inter-chain transfer integral becomes large. In $(TMTSF)_2PF_6$, the ground state is a $2k_F$ spin-density wave coexistent with a purely electronic, $2k_F$ charge-density wave:[25,26] the charge densities are modulated as rich, rich, poor, poor, … (period 4) as in the CDW phase of the MMX chains. The mechanism of the purely electronic, $2k_F$ charge-density wave is explained by the introduction of next-nearest-neighbor repulsion,[27] as in the present case of the MMX chains. As far as the charge degrees of freedom are concerned, the MMX chains and the quasi-one-dimensional organic conductors are similar in that chemical pressure induces a transition from the CP phase to the CDW phase. As to the spin degrees of freedom, the CP phase is paramagnetic, while the CDW phase is nonmagnetic, contrary to the spin-density-wave state of $(TMTSF)_2PF_6$.

## Site-diagonal *vs.* site-off-diagonal electron–lattice interactions

The ACP phase is found at low temperatures in $Pt_2(RCS_2)_4I$ ($R=CH_3$, $n$-$C_4H_9$),[11,12] where the MMX chains are neutral. There is no counter ion that acts as an obstacle to displacements of M atoms as in $R_4[Pt_2(pop)_4I]nH_2O$. Then, we set $K_{MXM}$ to be zero. To start with, we simply neglect the long-range interactions and study the competition between the site-diagonal ($\beta$) and site-off-diagonal ($\alpha$) electron–lattice couplings and the effect of the on-site repulsion $U_M$ on it. Exactly diagonalizing the one-band model, we show a phase diagram on the $\alpha$–$\beta$ plane in Fig. 6, where $t_{MM}$ is set to be unity, $t_{MXM}=0.8$, and $U_M=0$ at first. Though the present system without any electron–electron interaction can be solved for infinitely large system size, we use the same system size as before to make comparison easy. The specific value of $K_{MX}$ is again insignificant. When $\beta$ is small, the CDW phase is stable only for very small $\alpha$. As $\alpha$ increases, it is soon replaced by the ACP phase, where the binuclear units are dimerized. It is regarded as a spin-Peierls state because a singlet is formed on

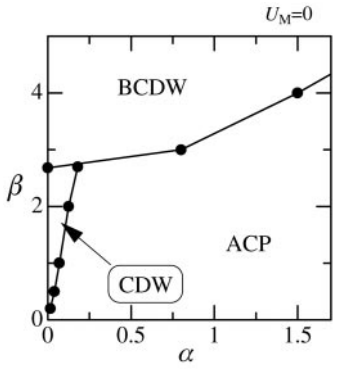


**Fig. 6** Ground-state phase diagram of the 12-site one-band model for $K_{MXM}=0$, on the $\alpha$–$\beta$ plane. The parameters are $t_{MM}=1$, $t_{MXM}=0.8$, $K_{MX}=6$, $U_M=0$, $V_{MM}=0$, $V_{MXM}=0$, and $V_2=0$.

the nearest-neighbor M sites accompanied with an X site in-between in the dimerized binuclear units. When both $\alpha$ and $\beta$ are small, the CDW phase is stabilized by $\beta$, if $\beta$ is not so large, because the CDW phase gains energy from the $\beta$ term, as described in the previous section, but the ACP phase does not. When $\beta$ is large enough, the BCDW phase appears because its energy gain from the $\beta$ term is the largest, as explained in the previous section.

In Fig. 7, we show how the on-site repulsion $U_M$ modifies the competition between the $\alpha$ and $\beta$ terms. For small or moderate $\alpha$ and $\beta$, the AV phase appears. As $U_M$ increases, all the phase boundaries are shifted to the large-$\beta$ side, and consequently the region of the AV phase is widened. This is because the on-site repulsion $U_M$ favors uniform charge densities, while the site-diagonal electron–lattice coupling $\beta$ favors modulation of

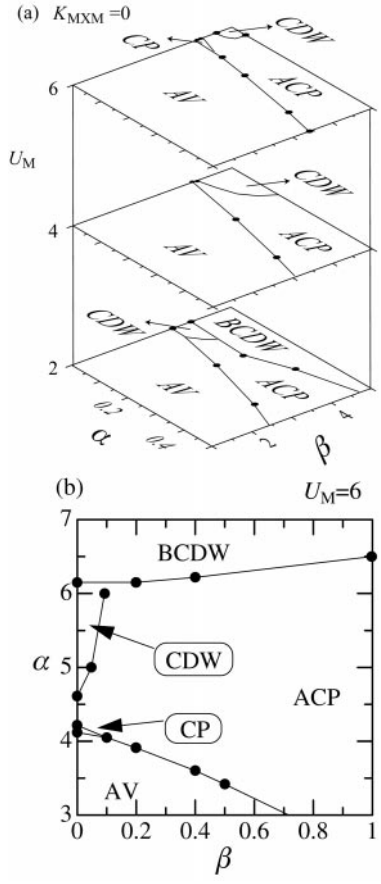


**Fig. 7** Ground-state phase diagram of the 12-site one-band model for $K_{MXM}=0$, (a) in the $\alpha$–$\beta$–$U_M$ space, and (b) its cross section at $U_M=6$. The parameters are $t_{MM}=1$, $t_{MXM}=0.8$, $K_{MX}=6$, $V_{MM}=0$, $V_{MXM}=0$, and $V_2=0$.

charge densities. Both terms compete with each other. Then, the BCDW phase is realized only when the $\beta$ term is strong enough to dominate over the $U_M$ term. The competition above is easily understood in the unphysical limit of small ionic mass. In this limit, the lattice displacements instantaneously follow the motion of electrons so that the $\beta$ term gives an attractive interaction to shift $U_M$ to $U_{M\,\mathrm{eff}} = U_M - \beta^2/K_{MX}$. This equation is derived from completing the squares with respect to variables $y_{a,i}$ and $y_{b,i}$. In the present limit of large ionic mass, however, the lattice displacements are statically shifted to form a bipolaron lattice, *i.e.*, the BCDW phase when $\beta$ is large enough. The situation becomes different when the site-off-diagonal electron–lattice coupling $\alpha$ increases. It favors modulation of bond-charge densities. The $U_M$ and $\alpha$ terms do not always compete with each other. In fact, they sometimes cooperate with each other when modulation of bond-charge densities is not accompanied with large modulation of (site-)charge densities.[28] That is why the phase boundaries are not shifted to the large-$\alpha$ side, but to the large-$\beta$ side, when $U_M$ increases. When $\alpha$ is large enough, the ACP phase is realized by modulating the distances between the neighboring binuclear units.

## Combined effects of the competitions above

Now we include the long-range interactions $V_{MM}$, $V_{MXM}$ and $V_2$: $V_{MM}=3$ and $V_2=2$ in addition to the parameters in Fig. 7(b), $U_M=6$. We show phase diagrams in Fig. 8(a) for $V_{MXM}=2$, and in Fig. 8(b) for $V_{MXM}=3$. The AV phase is destabilized by the long-range interactions, which favor modulation of charge densities in the purely electronic origin and compete with the on-site repulsion $U_M$. The ACP phase is realized in a wide parameter space. The nature of the ACP phase changes continuously from small-$\alpha$ to large-$\alpha$ ranges. For small $\alpha$, electrons are more localized, so that the singlet pair of

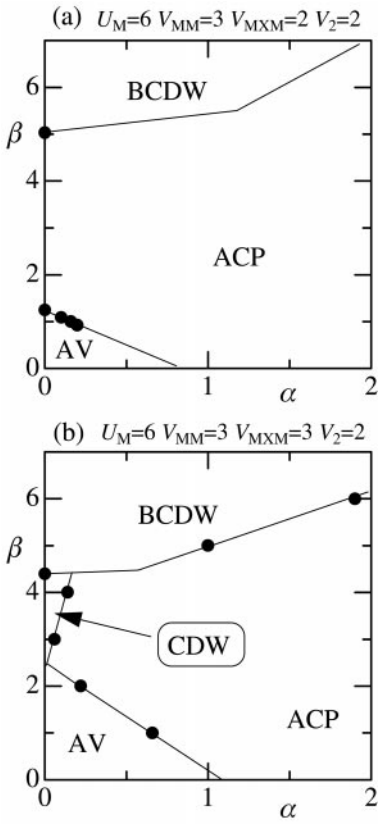


**Fig. 8** Ground-state phase diagrams of the 12-site one-band model for $K_{MXM}=0$, on the $\alpha$–$\beta$ plane, for (a) $V_{MXM}=2$, and (b) $V_{MXM}=3$. The parameters are $t_{MM}=1$, $t_{MXM}=0.8$, $K_{MX}=6$, $U_M=6$, $V_{MM}=3$, and $V_2=2$.

electrons are well described in the Heitler–London picture. For large $\alpha$, the neighboring M $d_{z^2}$ orbitals through the X $p_z$ orbital are strongly overlapped to form a doubly occupied bonding orbital, so that the electrons are as in a covalent molecule. Comparing Fig. 8(a) with Fig. 8(b), one sees that the nearest-neighbor repulsion through an X site, $V_{MXM}$, suppresses the ACP phase and stabilizes the other phases relative to the ACP phase, as already discussed through the aid of Fig. 5.

In recent experiments, the ACP phase is clearly observed in $Pt_2(n\text{-}C_4H_9CS_2)_4I$ below 200 K.[12] It is indeed nonmagnetic as expected in the ACP phase. The electronic structure of $Pt_2(CH_3CS_2)_4I$ is also suggested to be the ACP phase below 80 K, though the magnetic susceptibility does not drop at low temperatures.[11] Since the lattice displacements are very small in the latter case, this electronic state would be close to another paramagnetic phase such as the AV or CP phase. The CP phase is actually proposed above 80 K.[11] Because the spin excitation spectrum is gapless in the CP phase, it can generally gain more free energy than the ACP phase from the entropy term at high temperatures, so that it is possible from the theoretical viewpoint. The presence of the CP phase between the high-temperature AV phase and the low-temperature ACP phase is also reproduced in the Hartree–Fock approximation for a two-band model,[19] although the charge excitation spectra in the AV and CP phases are gapless owing to the approximation. Detailed studies of the finite-temperature CP phase in the dta system are left for the future since the electron correlation is essential for the charge gap. The X $p_z$ orbitals neglected in this section are expected to be quantitatively important for the "metallic" (*i.e.*, the resistivity increases with temperature) conductivity above 300 K (note that a small but finite gap is observed in the optical conductivity spectrum) and the small lattice displacements in the ACP phase.

We show phase diagrams containing all of the AV, ACP, CP, and CDW phases in Fig. 9, which are obtained by exactly diagonalizing the one-band model. Note that $K_{MXM}$ is not set to be zero or infinity here. These phase diagrams may become useful when experimental data are accumulated for the pop systems in future. The long-range interactions are weaker than those in Fig. 8. In Fig. 9(a), we use $t_{MM}=1$, $t_{MXM}=0.8$, $K_{MX}=6$, and $U_M=6$ as before. For small $\alpha$, as $\beta$ increases, the ground state changes from the AV phase, the CP phase, to the CDW phase, as in the case of infinitely large $K_{MXM}$. It finally becomes the BCDW phase for very large $\beta$ (not shown). For large enough $\alpha$, the ACP phase appears as usual. The critical strength of $\alpha$ for the ACP phase is the smallest at the boundary between the AV and CP phases. In Fig. 9(b), we change only $K_{MX}$ among the parameters of Fig. 9(a): $K_{MX}=4$. The MX bonds are more easily distorted by the smaller $K_{MX}$, while the distances between the neighboring binuclear units are almost unaffected because $K_{MXM}$ is not changed. Consequently, the CP and CDW phases are stabilized to shift the phase boundaries to the small-$\beta$ side, while the ACP phase is destabilized relative to these phases and invaded by them. In other words, some of the ACP states are replaced by the CDW states for the smaller $K_{MX}$. If we want to explain the difference between the pop and dta systems simply by the difference in $K_{MX}$ (not in $K_{MXM}$ as we do in this paper), we need larger $K_{MX}$ for the dta systems, contrary to intuition. In Fig. 9(c), we change only $t_{MXM}$ from the parameters of Fig. 9(a): $t_{MXM}=0.5$. The ACP phase is the most affected by this change and destabilized by the reduction of $t_{MXM}$. This is because the energy gain from forming a singlet pair of electrons (on the nearest-neighbor M sites accompanied by an X site in-between in the binuclear units) is proportional to $t_{MXM}^2$ and thus reduced. Meanwhile, the boundaries between the AV and CP phases and between the CP and CDW phases are not much affected by the change of $t_{MXM}$. It is not regarded as a main mechanism for the variation of the electronic phases in $R_4[Pt_2(pop)_4I]nH_2O$.

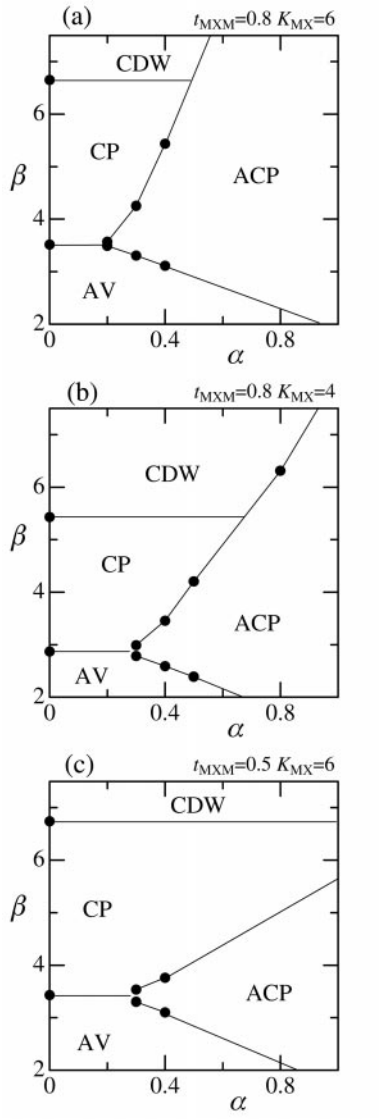


**Fig. 9** Ground-state phase diagrams of the 8-site one-band model for $K_{MXM}=1$, on the $\alpha$–$\beta$ plane, for (a) $t_{MXM}=0.8$, $K_{MX}=6$, (b) $t_{MXM}=0.8$, $K_{MX}=4$, and (c) $t_{MXM}=0.5$, $K_{MX}=6$. The parameters are $t_{MM}=1$, $U_M=6$, $V_{MM}=1.5$, $V_{MXM}=1$, and $V_2=0.5$.

## Inclusion of X $p_z$ orbitals

Here, we take X $p_z$ orbitals into account, using the two-band model. We do not focus on the features that appear only in the two-band model, *i.e.*, for small $(\varepsilon_M-\varepsilon_X+U_M-U_X)$. These features have already been discussed on the basis of Hartree–Fock calculations[15,16] and quantum Monte Carlo simulations.[22] We here aim at connection with the discussions below for the optical conductivity in the one- and two-band models. We will clarify the relation between these models. In this section, we neglect the long-range interactions for simplicity.

We estimate the effective magnitude of the inter-unit transfer integral $t_{MXM}$ in the two-band model. For simplicity, the $\alpha$ and $\beta$ terms are neglected and the energy levels are calculated in the isolated M–X–M system. From the level splitting, we have $t_{MXM}\sim[(\Delta_h^2+8t_{MX}^2)^{1/2}-\Delta_h]/4$ for the CDW and CP phases. As $\Delta_h$ decreases, $t_{MXM}$ increases, which corresponds to the order Cl < Br < I.

In $Pt_2(CH_3CS_2)_4I$, the X $p_z$ orbitals are suggested to be important for the high electric conductivity and the large deviation from double occupancy on the X sites.[11] We then set $K_{MXM}$ to be zero again and find the competition between the CDW and ACP phases and the absence of the CP phase. The findings are understood by using the second-order perturbation theory with respect to $t_{MM}$, and the fourth-order perturbation theory with respect to $t_{MX}$. For $K_{MXM}=0$, the energies of the CDW, ACP, and CP phases are all degenerate in the strong-coupling limit, $t_{MM}=t_{MX}=\alpha=0$, and given by $2\varepsilon_X-\beta|y|+U_M+U_X+K_{MX})y^2$ per binuclear unit. In the ACP phase, the energy gain from the intra-unit charge-transfer processes is the same as that in the CP phase, $t_{MM}^2/(2\beta|y|)$. Its energy gain from the MX charge-transfer processes is the same as those in the CDW and CP phases, $(t_{MX}+\alpha|y|)^2/(\Delta_h+\beta|y|)$. Therefore, the degeneracy of the ACP and CP phases is not lifted in the second order with respect to $t_{MM}$ and $t_{MX}$. However, in the fourth order with respect to $t_{MX}$, the spin-singlet ACP phase gains energy from the inter-unit charge-transfer processes by $2(t_{MX}+\alpha|y|)^4\{(1/U_M)+[2/(2\Delta_h+2\beta|y|+U_X)]\}/(\Delta_h+\beta|y|)^2$. Consequently, the CP phase is always higher in energy owing to the nearest-neighbor transfer integral strengthened by $\alpha$, so that it does not appear for $K_{MXM}=0$. As in the one-band model, the AV phase appears for small $\alpha$ and $\beta$, with the boundary shifted to the large-$\beta$ side with increasing $U_M$. The ACP phase stabilized by $\alpha$ is replaced by the CDW phase for large $\beta$. The region of the ACP phase is widened by $U_M$.

## Optical conductivity in the four-site model for XMMX monomers

We discussed possible mechanisms for the variation of the electronic phases in $R_4[Pt_2(pop)_4I]nH_2O$ in the previous sections. However, we cannot uniquely identify the mechanism until the model parameters are quantitatively evaluated. In this section, we discuss how to derive the magnitudes of the model parameters for X = Cl, Br, and I from the optical conductivity spectra. In general, there are still too many parameters to fit the spectra. In addition, approximations are unavoidable when calculating the spectra for MMX chains of infinite length. Fortunately, there are systems, $K_4[Pt_2(pop)_4X_2]nH_2O$ (X = Cl, Br, I), where XMMX units are almost isolated. The distances within the XMMX monomer are nearly equal to those in the $X–M^{3+}M^{3+}–X$ unit of the corresponding MMX chains (X = Cl, Br). Because the XMMX monomer consists of four sites, the exact spectrum is theoretically obtained for each set of parameters freely from any approximation. As demonstrated below, the optical conductivity spectra contain much information. From the dependence of the spectrum on the halogen ion, all peaks can be assigned. Then, we can considerably narrow the ranges for the magnitudes of the model parameters.

In recent optical conductivity measurements of $K_4[Pt_2(pop)_4X_2]nH_2O$ containing $X–M^{3+}M^{3+}–X$ monomers, three peaks are observed for each X.[8] They are ascribed to the charge-transfer processes between the M sites ($P_{MM}$), between the nearest-neighbor M and X sites ($P_{MX}$), and between the M and X sites with the remaining M site in-between ($P_{2MX}$). These processes are schematically shown in Fig. 10(a). The four-site model is explicitly written as

$$\begin{aligned}H_{XMMX}=-\sum_{\sigma}[&t_{MM}(c_{2\sigma}^{+}c_{3\sigma}+\text{h.c.})\\&+t_{MX}(c_{1\sigma}^{+}c_{2\sigma}+c_{3\sigma}^{+}c_{4\sigma}+\text{h.c.})\\&+t_{2MX}(c_{1\sigma}^{+}c_{3\sigma}+c_{2\sigma}^{+}c_{4\sigma}+\text{h.c.})]\\&+\varepsilon_M(n_2+n_3)+\varepsilon_X(n_1+n_4)\\&+U_M(n_{2\uparrow}n_{2\downarrow}+n_{3\uparrow}n_{3\downarrow})\\&+U_X(n_{1\uparrow}n_{1\downarrow}+n_{4\uparrow}n_{4\downarrow})\\&+V_{MM}n_2n_3+V_{MX}(n_1n_2+n_3n_4)\\&+V_{2MX}(n_1n_3+n_2n_4)\end{aligned}$$

where $c^{+}{}_{i\sigma}$ creates an electron with spin $\sigma$ at site $i$, h.c. denotes hermitian conjugate, $n_{i\sigma}=c^{+}{}_{i\sigma}c_{i\sigma}$, and $n_i=\Sigma_\sigma n_{i\sigma}$. Six electrons

are present in the four-site model. Here, we include the transfer integral and the repulsion strength for the next-nearest-neighbor M and X sites, $t_{2MX}$ and $V_{2MX}$, respectively. The real and finite-frequency part of the conductivity is proportional to the imaginary part of the current–current correlation function divided by frequency, $\omega$.

Before showing detailed results, we will give approximate relations between the energies and intensities of the three charge-transfer excitations. The ground state has even parity and is a spin-singlet, so that it is a linear combination of the six $^1$A states in Fig. 10(b). In the strong-coupling limit, $t_{MM}=t_{MX}=t_{2MX}=0$, the ground-state energy is given by $E_0=-2\Delta_h+V_{MM}$ when a constant term is so subtracted that the fully occupied state has zero energy. Here, the level difference in the hole picture is given by $\Delta_h=\varepsilon_M-\varepsilon_X+U_M-U_X+2V_{MM}$. Note that the formula of $\Delta_h$ depends on the coordination numbers, so that it is different from that for the MMX chains. The optically allowed, excited states have odd parity and are spin-singlets. There are four such $^1$B states, as shown in Fig. 10(b), though one of them has a negligible intensity. In the strong-coupling limit, the energies of the remaining three states are given by $E_{MX}=-\Delta_h+V_{2MX}$, $E_{MM}=-2\Delta_h+U_M$, and $E_{2MX}=-\Delta_h+V_{MX}$. Then, the excitation energies $\Delta E_v=E_v-E_0$ are given by

$$\Delta E_{MX}=V_{2MX}+\Delta_h-V_{MM}$$
$$\Delta E_{MM}=U_M-V_{MM}$$
$$\Delta E_{2MX}=V_{MX}+\Delta_h-V_{MM}$$

The intensities in the optical conductivity spectrum are proportional to $I_v=|<v|j|0>|^2/\Delta E_v$, where $|0>$ and $|v>$ are the ground and $v$th excited states, and $j$ is the paramagnetic current-density operator. The intensities are calculated in the lowest-order perturbation theory with respect to $t_{MX}$, $t_{MM}$, and $t_{2MX}$,

$$I_{MX}=2t_{MX}^2/\Delta E_{MX}$$
$$I_{MM}=4t_{MM}^2/\Delta E_{MM}$$
$$I_{2MX}=8t_{2MX}^2/\Delta E_{2MX}$$

From the equations for $\Delta E_v$ and $I_v$ in the strong-coupling limit, six parameters are independently estimated for each compound from the fitting to its optical conductivity spectrum, although

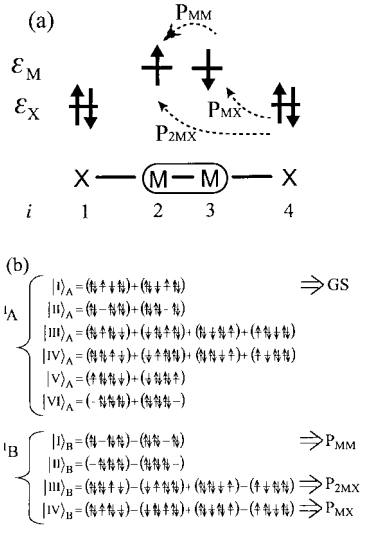


**Fig. 10** (a) Schematic electronic structure and charge-transfer excitations in the XMMX monomer, and (b) basis functions for the representation, $^1$A and $^1$B, corresponding to the ground and photo-excited states, respectively.

quantitative evaluation needs exact diagonalization. Namely, the energies $\Delta E_v$ give three repulsion strengths (plus a constant), $V_{2MX}+\Delta_h$, $U_M$, and $V_{MX}+\Delta_h$, relative to $V_{MM}$, while the intensities $I_v$ give the squares of the three transfer integrals, $t_{MX}$, $t_{MM}$, and $t_{2MX}$, divided by the respective excitation energies.

## Relation between parameters obtained from the optical conductivity

In the optical experiments of $K_4[Pt_2(pop)_4X_2]nH_2O$ (X=Cl, Br, I), many relations are found.[8] We will describe them below. First of all, from the dependence on the halogen atom X, the relation $\Delta E_{MX}<\Delta E_{MM}<\Delta E_{2MX}$ is reasonably derived from the fact that $\Delta E_{MM}$ should be the most insensitive to X among the three $\Delta E_v$, and $I_{MM}$ among the three $I_v$. The previous analysis of the excitation energies in the strong-coupling limit suggests that the relation

$$V_{2MX} < U_M-\Delta_h < V_{MX}$$

holds for $K_4[Pt_2(pop)_4X_2]nH_2O$ with X=Cl, Br, and I. The nearest-neighbor interactions are found to have substantial strengths. The charge-transfer energies between M and X sites, $\Delta E_{MX}$ and $\Delta E_{2MX}$, both increase with decreasing $X^-$ radius: $\Delta E_{PtI}<\Delta E_{PtBr}<\Delta E_{PtCl}$ and $\Delta E_{2PtI}<\Delta E_{2PtBr}<\Delta E_{2PtCl}$. For each X, the excitation intensity becomes larger with increasing excitation energy: $I_{MX}<I_{MM}<I_{2MX}$. The intensity of the lowest-energy excitation decreases with decreasing $X^-$ radius: $I_{PtI}>I_{PtBr}>I_{PtCl}$. Meanwhile, the intensity of the highest-energy excitation shows complex behavior, *i.e.*, it becomes the largest at X=Br: $I_{2PtI}<I_{2PtBr}$, $I_{2PtBr}>I_{2PtCl}$, and $I_{2PtI}\sim I_{2PtCl}$.

The level difference in the electron picture $\varepsilon_M-\varepsilon_X$ increases with decreasing $X^-$ radius: $\varepsilon_{Pt}-\varepsilon_I<\varepsilon_{Pt}-\varepsilon_{Br}<\varepsilon_{Pt}-\varepsilon_{Cl}$. If the on-site repulsion strength at X sites $U_X$ does not change as much as $\varepsilon_M-\varepsilon_X$, the level difference in the hole picture $\Delta_h$ also increases with decreasing $X^-$ radius. This would be one of the reasons for the relations $\Delta E_{PtI}<\Delta E_{PtBr}<\Delta E_{PtCl}$ and $\Delta E_{2PtI}<\Delta E_{2PtBr}<\Delta E_{2PtCl}$. The distance between the neighboring M and X sites $d_{MX}$ decreases with decreasing $X^-$ radius: $d_{PtI}>d_{PtBr}>d_{PtCl}$. It is then reasonable that $V_{MX}$ and $V_{2MX}$ increase with decreasing $X^-$ radius: $V_{PtI}<V_{PtBr}<V_{PtCl}$ and $V_{2PtI}<V_{2PtBr}<V_{2PtCl}$. Meanwhile, the distance between the neighboring M sites $d_{MM}$ is almost a constant for all X. Because the repulsion strengths $U_M$ and $V_{MM}$ should not change as much as $V_{MX}$ and $V_{2MX}$, these relations for $V_{MX}$ and $V_{2MX}$ also lead to the observed relations for $\Delta E_{MX}$ and $\Delta E_{2MX}$. If we assume that $t_{MX}$ does not change so much as $\Delta E_{MX}$, the above relation for $\Delta E_{MX}$ leads to the observed relation for $I_{MX}$, $I_{PtI}>I_{PtBr}>I_{PtCl}$. Meanwhile, the observed relation for $I_{2MX}$ is complex. This would be due to interference among the second-order process with respect to $t_{2MX}$ and the higher-order processes with respect to $t_{MX}$ and $t_{MM}$. In short, except the complex relation for $I_{2MX}$, the strong-coupling analysis explains the observed dependence of the energies and intensities on the halogen atom X.

From the exact diagonalization of the four-site two-band model for the XMMX monomers, we show the dependence of the energies $\Delta E_v$ and the intensities $I_v$ of the three charge-transfer excitations on the level difference $\varepsilon_M-\varepsilon_X$ in Fig. 11(a), on the long-range electron–electron interactions $V_{MX}$ and $V_{2MX}$ in Fig. 11(b), and on the transfer integrals $t_{MX}$ and $t_{2MX}$ in Fig. 11(c). As discussed above, the excitation energies $\Delta E_{MX}$ and $\Delta E_{2MX}$ are found to increase with $\varepsilon_M-\varepsilon_X$, $V_{MX}$, and $V_{2MX}$, while the energy $\Delta E_{MM}$ is insensitive to them. Meanwhile, the behavior of the excitation intensities is much more complex than that of the excitation energies: $I_v$ is not necessarily proportional to $1/\Delta E_v$. With increasing $t_{MX}$ and $t_{2MX}$, $I_{2MX}$ reasonably increases, but $I_{MX}$ does not increase so much, and furthermore $I_{MM}$ changes greatly. This is due to the

interference among the second- and higher-order processes with respect to the transfer integrals. In fact, when we take very small values for the transfer integrals, we of course reproduce the lowest-order relations for $I_\nu$ shown above. Consequently, it is rather easy to fit the parameters to the excitation energies, but not to the excitation intensities. In the optical experiments, all of the parameters, $\varepsilon_M-\varepsilon_X$, $V_{MX}$, $V_{2MX}$, $t_{MX}$, and $t_{2MX}$ change with X, leading to the non-monotonous dependence of $I_{2MX}$ on the $X^-$ radius. We can say, at least, the numerical factors 2, 4, and 8 for $I_{MX}$, $I_{MM}$, and $I_{2MX}$, respectively, are rather important for the relations $\Delta E_{MX}<\Delta E_{MM}<\Delta E_{2MX}$ and $I_{MX}<I_{MM}<I_{2MX}$ to be compatible with each other. In other words, we do not need a relation like $t_{MX}<t_{MM}<t_{2MX}$, in fact, to have $I_{MX}<I_{MM}<I_{2MX}$ in Fig. 11.

## Implication for the mechanism of the phase variation

Compared with any relation concerning the intensities, the relation derived above from the energies, $V_{2MX}<U_M-\Delta_h<V_{MX}$, is rather robust unless the transfer integrals are very large. This indicates substantial strengths of the nearest-neighbor repulsion $V_{MX}$ in the two-band model and of $V_{MXM}$ (at least for the $M^{3+}$–X–$M^{3+}$ unit of the ACP phase) in the one-band model. The intra-unit nearest-neighbor repulsion $V_{MM}$ would also be substantially strong. Therefore, we believe that the variety of the electronic phases in $R_4[Pt_2(pop)_4I]nH_2O$ originates from both the competition between the electron–lattice and electron–electron interactions and that between the short-range and long-range electron–electron interactions. As discussed in the following sections, the present scenario qualitatively explains the experimentally observed variation of the optical properties also.

Including the long-range repulsion strengths $V_{2MX}$, $V_{MXM}$, and $V_2$, we estimate the energies of the charge-ordered phases per binuclear unit in the strong-coupling limit, $t_{MM}=t_{MX}=t_{2MX}=t_{MXM}=\alpha=0$, of the two-band model ($\varepsilon_M=0$) as

$$E_{CDW}=E_1+(5/2)V_{MM}+2V_{MXM}+4V_2$$
$$E_{ACP}=E_1+2V_{MM}+(5/2)V_{MXM}+4V_2+2K_{MXM}y^2$$
$$E_{CP}=E_1+2V_{MM}+2V_{MXM}+5V_2$$

where

$$E_1=2\varepsilon_X-\beta|y|+U_M+U_X+6V_{MX}+6V_{2MX}+K_{MX}y^2$$

Of course, these energies are reduced to those in the one-band model in the limit of infinitely large $\varepsilon_M-\varepsilon_X$. For large $K_{MXM}$ and $V_{MM}$, the CP phase is the most stable in the limit. The relative stability between the CDW and CP phases is again discussed with the help of the second-order perturbation theory with respect to $t_{MM}$ and $t_{MXM}$. In the CDW phase, the energy gain from the intra-unit charge-transfer processes is $t_{MM}^2/(U_M-V_{MM})$ (in the spin-polarized state, or $2t_{MM}^2/(U_M-V_{MM})$ in the spin-singlet state), and that from the inter-unit processes is $t_{MXM}^2/(2\beta|y|-V_{MM}+2V_2)$. It is noted that the energy denominators presented here for the second-order corrections appear again in the context of charge-transfer excitations in the next section. In the CP phase, the energy gain from the intra-unit processes is $t_{MM}^2/(2\beta|y|+V_{MXM}-2V_2)$, and that from the inter-unit processes is $t_{MXM}^2/(2\beta|y|+V_{MM}-2V_2)$. Therefore, the CDW phase becomes stabilized when the site-diagonal electron–lattice coupling $\beta$ is strong enough. Note that the second-order terms with respect to $t_{MXM}$ for these phases are now different owing to the long-range interactions.

## Optical conductivity in the one-band model for MMX chains

We come back to the MMX chains and calculate the optical conductivity spectra. The low-energy excitations are now mainly caused by inter-unit collective charge-transfer processes. In fact, the optical absorption for the MMX chains of $K_4[Pt_2(pop)_4Br]nH_2O$ in the CDW phase containing the X–$M^{3+}M^{3+}$–X unit[29] takes place at a much lower energy than for the corresponding XMMX monomers of $K_4[Pt_2(pop)_4Br_2]nH_2O$.[8] So, we adopt the one-band model, having $R_4[Pt_2(pop)_4I]nH_2O$ in mind. Here, we focus on differences among the spectra in the AV, CDW, and CP phases. We do not calculate the lattice displacements self-consistently but fix them to be a constant, $|y|=y_0$, although we change the distortion pattern according to the electronic phase. The elastic constants are then meaningless. The lattice displacements are $y_{a,i}=y_{b,i}=0$ in the AV phase, $y_{a,i}=y_{b,i}=(-1)^i y_0$ in the CDW phase, and $y_{a,i}=-y_{b,i}=y_0$ in the CP phase. The optical excitation

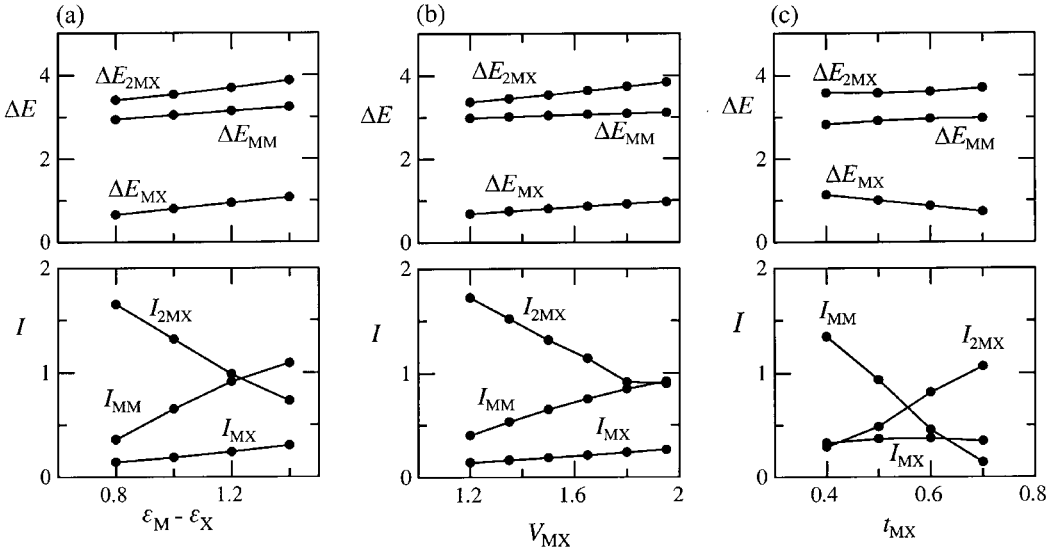


**Fig. 11** Energies $\Delta E_\nu$ and intensities $I_\nu$ of the photoexcitations as a function of (a) $\varepsilon_M-\varepsilon_X$ ($V_{MX}=1.5$, $V_{2MX}=0.5$, $t_{MX}=t_{2MX}=0.55$), (b) $V_{MX}$ and $V_{2MX}=V_{MX}/3$ ($\varepsilon_M-\varepsilon_X=1$, $t_{MX}=t_{2MX}=0.55$), and (c) $t_{MX}$ and $t_{2MX}=0.8t_{MX}$ ($V_{MX}=1.5$, $V_{2MX}=0.5$, $\varepsilon_M-\varepsilon_X=1$). The other parameters are $t_{MM}=1$, $U_M=2$, $U_X=4$, and $V_{MM}=1$.

processes are schematically represented in Fig. 12 for the CDW and CP phases. The illustration becomes realistic only near the strong-coupling limit. In this limit, the excitation energies in the CDW phase are given by

$$E_{MM}^{CDW} = U_M - V_{MM}$$
$$E_{MXM}^{CDW} = 2\beta|y| - V_{MM} + 2V_2$$

while those in the CP phase are given by

$$E_{MM}^{CP} = 2\beta|y| + V_{MXM} - 2V_2$$
$$E_{MXM}^{CP} = 2\beta|y| + V_{MM} - 2V_2$$

Among the four energies, $E^{CDW}{}_{MM}$ is expected to be much larger than the others because of the strong on-site repulsion $U_M$.

From the exact diagonalization of the one-band model, we show optical conductivity spectra in the three phases for $U_M=2$ in Fig. 13(a), for $U_M=4$ in Fig. 13(b), and for $U_M=6$ in Fig. 13(c), with varying $V_{MM}$ and $V_{MXM}$ according to the relations $V_{MM}=U_M/2$ and $V_{MXM}=U_M/4$. As the electron–electron interactions are not so weak, a single peak appears at a similar position in both of the AV and CDW phases, while two peaks generally appear in the CP phase, in the energy range of the figures. The difference in the number of peaks between the CDW and CP phases is due to the strong on-site repulsion $U_M$, as discussed above. We then focus on the CP phase and show the dependence of the energies and intensities of the two excitations on the long-range interactions $V_{MM}$ and $V_{MXM}$ in Fig. 14. The lower energy $E^{CP}{}_{MM}$ increases with $V_{MXM}$, while the higher energy $E^{CP}{}_{MXM}$ increases with $V_{MM}$, as expected from the strong-coupling analysis. The excitation intensities are comparable when the energy difference is small. Meanwhile, the low-energy excitation is much stronger when the energy difference is large.

In the optical experiments, so far all $R_4[Pt_2(pop)_4I]nH_2O$ compounds have a single peak below 3 eV.[8] Observation of a single peak is reasonable in the phase suggested to be the AV phase and in the CDW phases because of the strong on-site repulsion $U_M$. Meanwhile, observation of a single peak in the phase suggested to be the CP phase indicates that the nearest-neighbor repulsion through an X site $V_{MXM}$ is substantially weaker (at least for the $M^{3+}$–X–$M^{2+}$ unit of the CP phase) than the nearest-neighbor repulsion within the unit $V_{MM}$. Recall that, in the XMMX monomers, substantially strong $V_{MX}$, and consequently strong $V_{MXM}$ for the $M^{3+}$–X–$M^{3+}$ unit, are suggested from the optical conductivity. It is quite possible for the repulsion $V_{MXM}$ to depend on the inter-unit distance $d_{MXM}$ rather sensitively, though we do not take account of this effect in order not to make the model more complex. We can say at least that the repulsion $V_{MM}$ is very strong, which is actually needed to stabilize the CP phase.

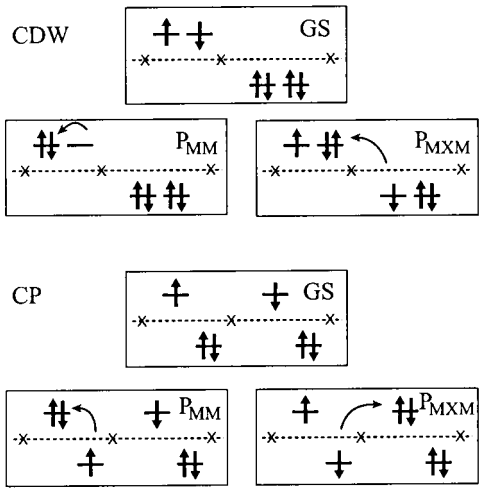


**Fig. 12** Schematic electronic structure and charge-transfer excitations in the CDW and CP phases of the one-band model.

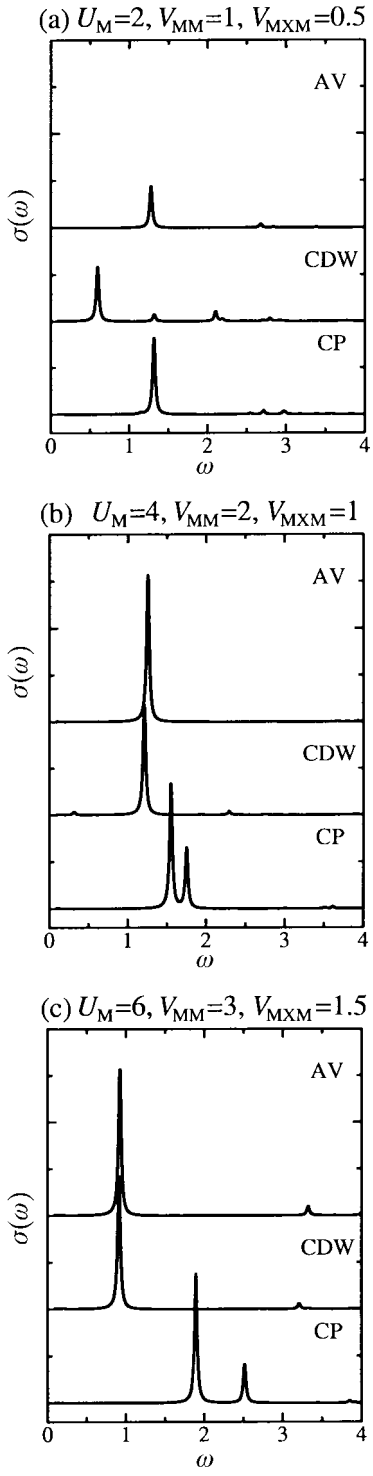


**Fig. 13** Optical conductivity in the AV, CDW, and CP phases of the 12-site one-band model, for (a) $U_M=2$, $V_{MM}=1$, $V_{MXM}=0.5$, (b) $U_M=4$, $V_{MM}=2$, $V_{MXM}=1$, and (c) $U_M=6$, $V_{MM}=3$, $V_{MXM}=1.5$. The other parameters are $t_{MM}=1$, $t_{MXM}=0.8$, $\alpha=0.2$, $\beta=4$, $y_0=0.1$, and $V_2=0$.

Among the energies of the experimentally observed peaks, that in the CDW phase is lower than those in the phase suggested to be the CP phase. The energy difference between the CDW and CP phases is reproduced in Fig. 13 for each

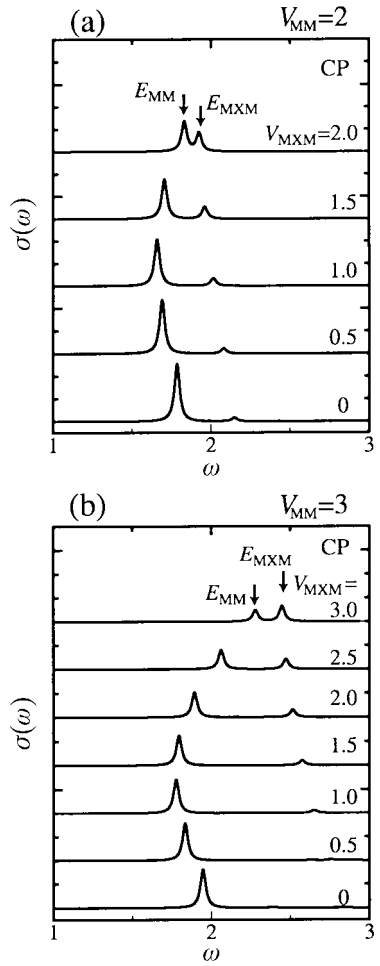


**Fig. 14** Optical conductivity in the CP phase of the 12-site one-band model, as a function of $V_{MXM}$, for (a) $V_{MM}=2$, and (b) $V_{MM}=3$. The parameters are $t_{MM}=1$, $t_{MXM}=0.8$, $\alpha=0.2$, $\beta=4$, $y_0=0.1$, $U_M=6$, and $V_2=0$.

parameter set. This is easily understood in the strong-coupling limit. The low-energy charge-transfer excitation takes place at $E^{CDW}{}_{MXM}=2\beta|y|-V_{MM}+2V_2$ in the CDW phase, and at $E^{CP}{}_{MM}=2\beta|y|+V_{MXM}-2V_2$ in the CP phase. We concluded above that the nearest-neighbor repulsion through an X site $V_{MXM}$ is substantially weaker, at least for the CDW and CP phases, than the nearest-neighbor repulsion within the unit $V_{MM}$. Furthermore, we reasonably expect that the next-nearest-neighbor repulsion $V_2$ is smaller than $V_{MXM}$. Therefore, we can derive the relation $E^{CDW}{}_{MXM}<E^{CP}{}_{MM}$, which explains the observed energy difference between the CDW and CP phases. This relation is intuitively understood in the following way. In the CDW phase, holes reside at $M^{3+}M^{3+}$ units. By any charge-transfer process, the hole pair in a unit is so separated that an electron and a hole attract each other by

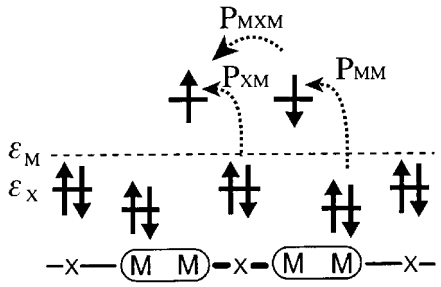


**Fig. 15** Schematic electronic structure and charge-transfer excitations in the ACP phase of the two-band model.

the amount of $V_{MM}$. In the CP phase, however, holes are so located that the distance between the neighboring holes is the largest among the possible electronic structures. By any charge-transfer process, some pairs of holes approach each other, so that it costs repulsive energy.

## Optical conductivity in the two-band model for MMX chains

We now employ the two-band model to discuss the optical conductivity spectrum in $Pt_2(CH_3CS_2)_4I$, where the X $p_z$ orbitals are generally expected to be located at a shallow position and to contribute to the electrical and optical conductivity. Here, we focus on the dependence of the spectrum on the model parameter governing the itinerant character of electrons, $t_{MX}$. Again, we do not calculate the lattice displacements self-consistently but fix them to be a constant, $|y|=y_0$. We consider the ACP phase observed in $Pt_2(RCS_2)_4I$ (R = $CH_3$, $n$-$C_4H_9$), using $y_{a,i}=-y_{b,i}=(-1)^i y_0$. The optical excitation processes are schematically represented in Fig. 15 for the ACP phase. Though the itineracy of electrons in $Pt_2(RCS_2)_4I$ is higher than that in $R_4[Pt_2(pop)_4I]nH_2O$, we first analyze the excitation energies in the strong-coupling limit. The charge-transfer process from an X site to the neighboring M site $P_{XM}$ costs energy, $E^{ACP}{}_{XM}=\Delta_h+\beta|y|+V_{MX}$, where the level difference in the hole picture is now given by $\Delta_h=\varepsilon_M-\varepsilon_X+U_M-U_X+2V_{MM}-2V_{MX}$. Note that this equation is different from that in the four-site model because the coordination numbers are different. The charge-transfer process within a binuclear unit $P_{MM}$ costs energy, $E^{ACP}{}_{MM}=2\beta|y|$, in the strong-coupling limit. In the optical experiment for $Pt_2(CH_3CS_2)_4I$, the peaks are so assigned that the relation $E_{XM}<E_{MM}$ is satisfied.[11] Precisely speaking, an M d orbital different from the $d_{z^2}$ orbital may be involved, but this relation is not modified in any case. This relation indicates $\Delta_h+V_{MX}<\beta|y|$, *i.e.*, substantial reduction of the level difference in the hole picture $\Delta_h$ and of the nearest-neighbor repulsion $V_{MX}$ in comparison with rather small $\beta|y|$ due to the small lattice distortion. However, $V_{MX}$ need not be so small, as shown below for large $t_{MM}$. From this fact, it is clear that the strong-coupling analysis does not work for $Pt_2(RCS_2)_4I$.

From the exact diagonalization of the two-band model, we show optical conductivity spectra in the ACP phase with varying $t_{MX}$ in Fig. 16. For small $t_{MX}$, three peaks corresponding to the three charge-transfer processes in Fig. 15 appear distinctly. The parameters are chosen to satisfy the relation $E_{MXM}<E_{XM}<E_{MM}$, as assigned in the experiment for $Pt_2(CH_3CS_2)_4I$.[11] Since the transfer integral $t_{MM}$ is not so

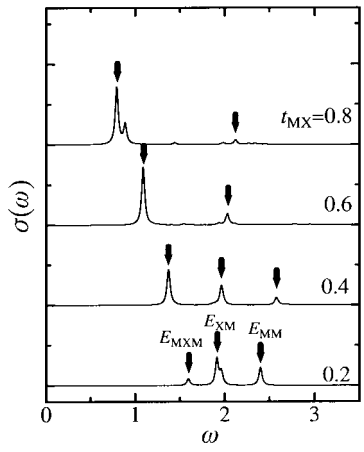


**Fig. 16** Optical conductivity in the ACP phase of the 18-site two-band model, as a function of $t_{MX}$. The parameters are $t_{MM}=1$, $\alpha=1$, $\beta=4$, $y_0=0.1$, $\varepsilon_M-\varepsilon_X=0.2$, $U_M=4$, $U_X=4$, $V_{MM}=2$, and $V_{MX}=2$.

small, the previous estimation of $E_{XM}$ and $E_{MM}$ does not work. Indeed, in Fig. 16, the used values for $\Delta_h$, $\beta$, and $V_{MX}$ do not satisfy the relation $E^{ACP}{}_{XM} < E^{ACP}{}_{MM}$ for the strong-coupling limit, but they actually satisfy the relation $E_{XM} < E_{MM}$ in the spectra. This means that $V_{MX}$ need not be so small as suggested by the strong-coupling analysis. As the transfer integral between the neighboring M and X sites $t_{MX}$ increases, the intensities of $P_{XM}$ and $P_{MM}$ decrease rapidly, and the spectral weight is concentrated on the inter-unit charge-transfer excitation $P_{MXM}$. At the same time, only this excitation substantially lowers its energy, reflecting the itinerant nature for large $t_{MM}$ and $t_{MX}$. In the experiment of $Pt_2(CH_3CS_2)_4I$, the lowest-energy excitation has a much larger intensity and a much lower energy than the other two excitations,[11] as in Fig. 16 for large $t_{MX}$.

## Conclusion

We theoretically study the variety of charge and lattice ordered phases and their respective optical responses in one-dimensional correlated-electron–lattice systems. One- and two-band models are used for the MMX chains and a four-site two-band model for the XMMX monomers. We use the exact diagonalization method to obtain the numerical results. The second- and fourth-order perturbation theories with respect to the transfer integrals as well as the strong-coupling analysis are found to be very useful in many cases, though not always, to understand the variation of the electronic phases and the respective optical conductivity spectra. Various terms in the model Hamiltonians compete with one another: the kinetic term controlled by transfer integrals, site-diagonal and site-off-diagonal electron–lattice interactions, short-range and long-range electron–electron interactions, and the elastic energies controlling the modulation of the MX bond lengths and that of the inter-unit distances.

A variety of electronic phases appear in $R_4[Pt_2(pop)_4I]nH_2O$, depending on the counter ion and on the number of water molecules. It is suggested from experiments that the electronic phases are classified according to the distance between the neighboring binuclear units $d_{MXM}$.[8] The AV phase is suggested to appear for small $d_{MXM}$. This phase is ascribed to the enhanced kinetic term by the large inter-unit transfer integral. For larger $d_{MXM}$, the CDW and CP phases compete with each other. The CP phase is suggested to appear for large $d_{MXM}$, while the CDW phase is realized between the other two phases. The relative stability between the CDW and CP phases is determined by a combined effect of competition between electron–lattice and electron–electron interactions and competition between short-range and long-range electron–electron interactions. As $d_{MXM}$ decreases, the site-diagonal electron–lattice interaction and long-range electron–electron interactions become larger, and their effects become dominant over the effect of the short-range electron–electron interaction. Thus the CP phase is reasonably converted to the CDW phase. The optical conductivity spectrum changes accordingly.

To evaluate the relative importance between the two types of competition above, we need quantitative estimation of the model parameters. For this purpose, we study the optical conductivity spectra of $K_4[Pt_2(pop)_4X_2]nH_2O$ containing almost isolated $X–M^{3+}M^{3+}–X$ monomers. Corresponding MMX chain compounds, $K_4[Pt_2(pop)_4X]nH_2O$ with X = Cl and Br, are fortunately in the CDW phase consisting of repeating $X–M^{3+}M^{3+}–X$ and $M^{2+}M^{2+}$ units. The dependence of the energies and intensities of three charge-transfer excitations in the XMMX monomers are reproduced by appropriate choice of the level difference, the repulsive strengths between electrons at M and X sites, and the transfer integrals between M and X orbitals. From the fitting to the experimentally observed spectra, we find substantially strong nearest-neighbor repulsion between the neighboring M and X sites. Consequently, the two types of competition are both quantitatively important and combined.

In $Pt_2(RCS_2)_4I$, the electric conductivity is rather high.[11] The itinerant character of electrons is much stronger than in the pop systems. The main difference between the two systems is that MMX chains in $R_4[Pt_2(pop)_4I]nH_2O$ are charged while those in $Pt_2(RCS_2)_4I$ are neutral. The former systems need to have counter ions, which prohibit free modulation of the distances between the neighboring binuclear units. This strongly suppresses the appearance of the ACP phase. On the other hand, the latter systems do not have counter ions so that the distances between the neighboring binuclear units are easily modulated by sufficiently strong site-off-diagonal electron–lattice coupling. As a consequence, the ACP phase appears. From the optical conductivity spectrum also, it is evident that the transfer integrals are large and electrons are more delocalized than in the pop systems. Though the electric conductivity shows metallic behavior in $Pt_2(CH_3CS_2)_4I$ above room temperature, where the lattice is not distorted, the optical conductivity spectrum shows a small but finite charge gap.[11] This AV phase as well as the AV phase suggested in $R_4[Pt_2(pop)_4I]nH_2O$ for small $d_{MXM}$ is then regarded as a Mott–Hubbard insulator phase.

## Acknowledgements

We are grateful to H. Kitagawa and H. Okamoto for showing their experimental data prior to publication and for thorough and enlightening discussions. This work was supported by a Grant-in-Aid for Scientific Research on Priority Area "Metal-Assembled Complexes" from the Ministry of Education, Science, Sports and Culture, Japan, a Grant-in-Aid for Scientific Research (C) from the Japan Society for the Promotion of Science, and the NEDO International Joint Research Grant Program. It is our great pleasure to dedicate this work to Professor A. E. Underhill on the occasion of his retirement from the University of Wales. We sincerely appreciate his pioneering work in metal complexes, which has indirectly but strongly influenced our theoretical research activities and brought us a fruitful outcome.

## References

1 H. Okamoto and M. Yamashita, *Bull. Chem. Soc. Jpn.*, 1998, **71**, 2023 and references therein.
2 M. Kurmoo and R. J. H. Clark, *Inorg. Chem.*, 1985, **24**, 4420.
3 L. G. Butler, M. H. Zietlow, C.-M. Che, W. P. Schaefer, S. Sridhar, P. J. Grunthaner, B. I. Swanson, R. J. H. Clark and H. B. Gray, *J. Am. Chem. Soc.*, 1988, **110**, 1155.
4 M. Yamashita and K. Toriumi, *Inorg. Chim. Acta*, 1990, **178**, 143.
5 J. B. Weinrach, M. Hawley, A. P. Sattelberger and B. I. Swanson, *Solid State Commun.*, 1991, **77**, 853.
6 N. Kimura, H. Ohki, R. Ikeda and M. Yamashita, *Chem. Phys. Lett.*, 1994, **220**, 40.
7 M. Yamashita, S. Miya, T. Kawashima, T. Manabe, T. Sonoyama, H. Kitagawa, T. Mitani, H. Okamoto and R. Ikeda, *J. Am. Chem. Soc.*, 1999, **121**, 2321.
8 H. Matsuzaki, H. Kishida, H. Okamoto, T. Kawashima, K. Takizawa, T. Ishii, T. Ono and M. Yamashita, *Meeting Abstr. Phys. Soc. Jpn.*, 2000, **55**, 744.
9 C. Bellitto, A. Flamini, L. Gastaldi and L. Scaramunzza, *Inorg. Chem.*, 1983, **22**, 444.
10 H. Kitagawa, N. Onodera, J.-S. Ahn, T. Mitani, K. Toriumi and M. Yamashita, *Synth. Met.*, 1997, **86**, 1931.
11 H. Kitagawa, N. Onodera, T. Sonoyama, M. Yamamoto, T. Fukawa, T. Mitani, M. Seto and Y. Maeda, *J. Am. Chem. Soc.*, 1999, **121**, 10068.
12 H. Kitagawa, Y. Iso, T. Mitani, M. Mitsumi and K. Toriumi, *Meeting Abstr. Phys. Soc. Jpn.*, 2000, **55**, 743.
13 M.-H. Whangbo and E. Canadell, *Inorg. Chem.*, 1986, **25**, 1726.
14 S. A. Borshch, K. Prassides, V. Robert and A. O. Solonenko, *J. Chem. Phys.*, 1998, **109**, 4562; V. Robert, S. Petit and S. A. Borshch, *Inorg. Chem.*, 1999, **38**, 1573.

15 S. Yamamoto, *Phys. Lett. A*, 1999, **258**, 183; S. Yamamoto, *Phys. Lett. A*, 1999, **261**, 125(E).
16 S. Yamamoto, *J. Phys. Soc. Jpn.*, 2000, **69**, 13.
17 M. Kuwabara and K. Yonemitsu, *Mol. Cryst. Liq. Cryst.*, 2000, **341**, 533.
18 M. Kuwabara and K. Yonemitsu, *Physica B*, 2000, **284–288**, 1545.
19 S. Yamamoto, *J. Phys. Soc. Jpn.*, 2001, **70**, 1198.
20 M. Kuwabara and K. Yonemitsu, *Mol. Cryst. Liq. Cryst.*, 2000, **343**, 47.
21 M. Kuwabara and K. Yonemitsu, *J. Phys. Chem. Solids*, 2001, **62**, 435.
22 S. Yamamoto, *Phys. Rev. B*, 2001, **63**, 125124.
23 D. Jérome, *Science*, 1991, **252**, 1509.
24 J. Moser, M. Gabay, P. Auban-Senzier, D. Jérome, K. Bechgaard and J. M. Fabre, *Eur. Phys. J. B*, 1998, **1**, 39.
25 J. P. Pouget and S. Ravy, *Synth. Met.*, 1997, **85**, 1523.
26 S. Kagoshima, Y. Saso, M. Maesato, R. Kondo and T. Hasegawa, *Solid State Commun.*, 1999, **110**, 479.
27 N. Kobayashi, M. Ogata and K. Yonemitsu, *J. Phys. Soc. Jpn.*, 1998, **67**, 1098.
28 K. Yonemitsu, A. R. Bishop and J. Lorenzana, *Phys. Rev. Lett.*, 1992, **69**, 965; K. Yonemitsu, A. R. Bishop and J. Lorenzana, *Phys. Rev. B*, 1993, **47**, 8065; K. Yonemitsu, A. R. Bishop and J. Lorenzana, *Phys. Rev. B*, 1993, **47**, 12059.
29 H. Okamoto, personal communication.